International Journal of Solids and Structures 51 (2014) 2687–2695

Contents lists available at ScienceDirect

International Journal of Solids and Structures

journal homepage: www.elsevier.com/locate/ijsolstr

# Prediction of the effective elastic moduli of materials with irregularly-shaped pores based on the pore projected areas

Borys Drach [a,*], Andrew Drach [b], Igor Tsukrov [c]

[a] Department of Mechanical & Aerospace Engineering, New Mexico State University, Las Cruces, NM, USA
[b] Institute for Computational Engineering and Sciences, University of Texas at Austin, Austin, TX, USA
[c] Mechanical Engineering Department, University of New Hampshire, Durham, NH, USA

ARTICLE INFO

*Article history:*
Received 7 October 2013
Received in revised form 21 March 2014
Available online 12 April 2014

*Keywords:*
Stochastic approach
Effective elastic moduli
Irregular pores
Micromechanical modeling

ABSTRACT

Statistical modeling is used to correlate geometric parameters of pores with their contributions to the overall Young's moduli of linearly elastic solids. The statistical model is based on individual pore contribution parameters evaluated by finite element simulations for a small pore subset selected using the design of experiments approach, so there is no need to solve the elasticity problem for all pores in the material. A polynomial relating pore geometric parameters to the contribution parameters is then fitted to the results of the simulations. We found a good correlation between normalized projected areas of the pores on three coordinate planes and their contributions to the corresponding effective Young's moduli. The model is applied and validated for two large sets of pore geometries obtained by X-ray microcomputed tomography of a carbon/carbon and a 3D woven carbon/epoxy composite specimens.



## 1. Introduction

Effective stiffness of linear elastic solids is reduced by the presence of pores. Historically, this reduction has been quantified in terms of the relative volume fraction of pores (porosity) assuming all pores to be spherical, see Dewey (1947), Mackenzie (1950). Later, the pore shapes were included in consideration by utilizing the famous Eshelby solution (Eshelby, 1957, 1959) for ellipsoidal inclusions and modeling non-spherical pores as ellipsoids of various eccentricities, see Wu (1966) and discussions in Kachanov et al. (1994) and David and Zimmerman (2011). For two-dimensional pores, in addition to circular and elliptical shapes, the analytical solutions for various quazi-polygonal holes have been utilized, see Zimmerman (1986), Tsukrov and Kachanov (1993), Jasiuk et al. (1994), Kachanov et al. (1994), Ekneligoda and Zimmerman (2006, 2008b), Zou et al. (2010). In three-dimensional case, only a limited number of analytical solutions for non-ellipsoidal inhomogeneities are available, including cuboids (Lee and Johnson, 1978), polyhedra (Rodin, 1996; Nozaki and Taya, 1997; Lubarda and Markenscoff, 1998), and superspherical shapes (Onaka, 2001; Hashemi et al., 2009; Sevostianov and Giraud, 2012) To evaluate contributions of pores having irregular shapes, when no analytical solution for a given shape is available, various numerical techniques, such as finite element or boundary element analyses, can be used.

Direct micromechanical modeling is the preferred way to predict effective elastic properties of materials with pores (with other possibilities being variational bounds on a property as in Hashin and Shtrikman, 1962 and later publications, or finite element simulations for the entire representative volume element with many pores as in Roberts and Garboczi (2000), Arns et al. (2002) and González et al. (2004)). It involves evaluation of contribution of a certain pore type to the effective elastic properties by solving the elasticity problem for a pore of that type, and then incorporating the solution into a certain micromechanical method. For irregular pore shapes, the elasticity problem is usually solved numerically. However, actual microstructures may contain large numbers of diverse pore shape types, and solving elasticity problems for all of them with reasonable accuracy may become computationally challenging and practically impossible.

It is therefore desirable to be able to evaluate how irregularly shaped pores influence the effective material properties without having to solve the elasticity problem. For this purpose, researchers have been trying to identify the appropriate geometric parameters (in addition to the overall porosity of the material) to be used for the predictions of effective properties.

* Corresponding author. Address: Mechanical & Aerospace Engineering, P.O. Box 30001/MSC 3450, New Mexico State University, Las Cruces, NM 88003-8001, USA. Tel.: +1 (575) 646 8041; fax: +1 (575) 646 6111.
*E-mail addresses:* borys@nmsu.edu (B. Drach), andrew.drach@utexas.edu (A. Drach), igor.tsukrov@unh.edu (I. Tsukrov).

http://dx.doi.org/10.1016/j.ijsolstr.2014.03.042
0020-7683/

Zimmerman (1991), for example, showed that compressibility of 2D pores correlates well with the undimensionalized ratio of pore perimeter $\Pi$ to its area $A$ defined as $\Pi^2/A$ (a three-dimensional analog of this parameter, the surface-to-volume ratio, was used in the stochastic model of Drach et al., 2013). Zimmerman's observation was later supported by numerical studies on several irregular 2D shapes (Tsukrov and Novak, 2002). However, such a parameter cannot be considered universal. For example, substitution of smooth pore boundaries by the very jagged ones (as illustrated in Fig. 1) will significantly increase the surface-to-volume ratio without making big changes in the overall response. This immediately follows from the comparison (or "auxiliary") theorem of Hill (1965) as interpreted by Kachanov and Sevostianov (2005). According to their interpretation, contributions of two pores with very different surface-to-volume ratios shown by solid lines in Fig. 1 are bounded by the same contributions of pores shown with dashed lines. The influence of corrugated boundaries on the overall compressibility of pores is also discussed in Ekneligoda and Zimmerman (2008a).

Another possible set of geometric parameters to characterize contribution of a pore to the effective elastic properties is its principal moments of inertia (PMIs). PMIs are defined as the eigenvalues of the matrix of moments of inertia given by $I_{ij} = \int_V \rho(\mathbf{r})(r^2\delta_{ij} - x_i x_j)dV$, where $\rho(\mathbf{r})$ is the material density of the body for which PMIs are calculated (pores can be treated as homogeneous bodies with $\rho(\mathbf{r}) = \rho = 1$), $r$ is the distance to the axis around which the moment is calculated, $\delta_{ij}$ is the Kronecker delta, $x_i$ are the coordinates $x_1, x_2, x_3$. PMIs have been previously used to approximate pores by the equivalent ellipsoids (Li et al., 1999; Drach et al., 2013). In Drach et al. (2013) we utilized statistical approaches to correlate pore principal moments of inertia to their contribution to the effective elastic moduli.

In this paper we investigate the hypothesis that contribution of irregularly-shaped pores to the effective Young's moduli of porous material can be evaluated based on their projected areas ("shadows") by statistical analysis of effective compliance parameters. We begin by selecting a certain subset of pores from the full dataset. Then, we perform finite element (FE) simulations for the pores in the subset to quantify their individual contributions to the effective compliance of the material. This data is then used in regression analysis to construct an approximating polynomial model for the dependence of pore's contribution to the effective compliance on its projected area. To verify that the model works for the full dataset, the constructed model is then checked against the FE simulations on the new subset of randomly chosen irregular shapes not used in the model fitting.

Because the accuracy of the model predictions (width of the error bars) depends on the number of direct simulations used in the data fitting, it is important to choose an "optimal" subset which corresponds to the desired model prediction variance. We use the design of experiments (DoE) approach (Ryan, 2007; Myers et al., 2009) to identify the list of input parameters (in our case, pore shape geometric parameters) that corresponds to the specified level of model prediction variance across the whole parameter space. We design the "experiment" (the combination of irregular shapes for FE simulations) using an I-optimal design module in JMP software (SAS Institute Inc, 2010). The optimization criterion for I-optimal designs is minimization of the integrated variance of the model predictions over the entire design space. This means that the expected width of confidence intervals for model predictions will be approximately the same across the full parameter space.

We apply this method to two sets of pore shapes obtained by microcomputed tomography of two different material samples: carbon/carbon and 3D woven carbon/epoxy composites. The examples of pore shapes are given in Fig. 2. For both sets we compare contributions of the pores to effective elastic properties determined by the direct FEA simulations for each pore with the ones based on its projected areas. Note that we use these sets of pore shapes only to check the hypothesis that statistical estimates based on the projected areas can be used instead of elasticity solutions. Our predictions cannot be directly used for carbon/carbon and 3D woven carbon/epoxy composites, because in our analysis we assume the pores to be placed in an isotropic homogeneous material which is obviously not the case for these composites. However, we feel that the considered pore shape sets provide good data to test the hypothesis, as the pores in these two cases result from very different mechanical processes (porosity from incomplete filling by chemical vapor deposition of pyrolytic carbon vs. damage due to chemical and thermal shrinkage of epoxy) and thus have different morphologies and shape distributions.

## 2. Micromechanical modeling approach utilizing statistical analysis

Characterization of individual pore contributions to the effective material response is based on the pore compliance contribution tensor – $\mathbf{H}$ -tensor proposed in Kachanov et al. (1994). Note that a similar tensor in the context of a microcrack was earlier given by Horii and Nemat-Nasser (1983). The fourth rank tensor $\mathbf{H}$ is defined as a set of proportionality coefficients between remotely applied homogeneous stress field $\boldsymbol{\sigma}_0$ and the additional strain $\Delta\boldsymbol{\varepsilon}$ generated in the material due to the presence of a cavity:

$$\Delta\boldsymbol{\varepsilon} = \mathbf{H} : \boldsymbol{\sigma}_0 \tag{1}$$

where ":" denotes the contraction over two indices. For a material with a large number of pores, a proper representative volume element (RVE) (Hill, 1963; Nemat-Nasser and Hori, 1999) can be selected, and the effective compliance tensor of the material is given by

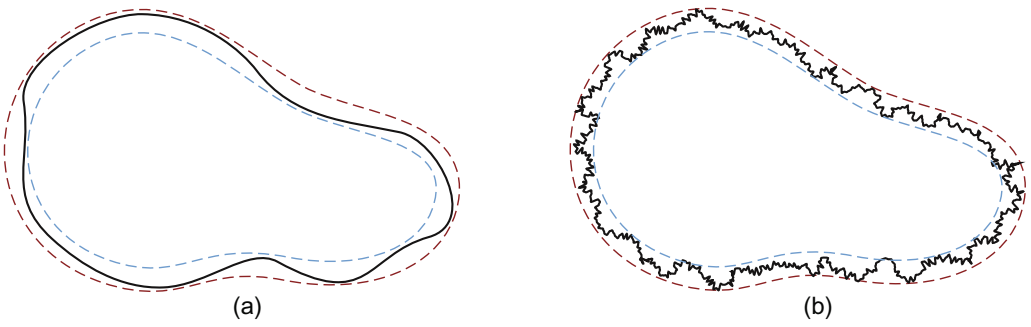


**Fig. 1.** Two pores having similar contributions to the overall elastic properties but significantly different surface-to-volume ratios. Dashed lines show upper and lower limits of their contributions.

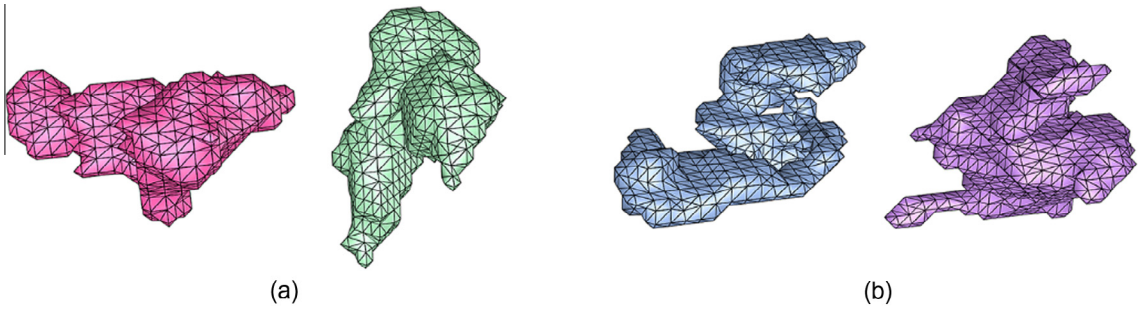


**Fig. 2.** Examples of pores extracted by microcomputed tomography from (a) carbon/carbon composite sample; (b) 3D woven carbon/epoxy composite sample.

$$\mathbf{S} = \mathbf{S}_0 + \mathbf{H}_{RVE}$$

where $\mathbf{S}_0$ is the compliance tensor of the matrix material and $\mathbf{H}_{RVE}$ is the contribution from all pores present in the RVE.

For dilute distribution of pores, the non-interaction approximation can be used, and $\mathbf{H}_{RVE}$ is found by direct summation of contributions from all individual pores in the RVE:

$$\mathbf{H}^{NI}_{RVE} = \sum_i \mathbf{H}_{(i)} \tag{2}$$

where $\mathbf{H}_{(i)}$ is the compliance contribution tensor of the $i$th pore. For higher porosities when the non-interaction approximation is no longer applicable, more advanced micromechanical schemes should be used. However, most of the first order micromechanical schemes can be readily expressed in terms of the non-interaction approximation, see Eroshkin and Tsukrov (2005). For example, predictions for the overall pore compliance contribution tensor by the Mori–Tanaka method (Mori and Tanaka, 1973; Benveniste, 1987) in terms of $\mathbf{H}^{NI}_{RVE}$ is given by a simple formula Kachanov et al. (1994):

$$\mathbf{H}^{MT}_{RVE} = \mathbf{H}^{NI}_{RVE}/(1-p) \tag{3}$$

where $p$ is the volume fraction of pores. The formulae for the effective Young's moduli in the next paragraph are given in the assumption of the non-interaction approximation but can be converted to other micromechanical schemes if needed.

To relate the pore compliance contribution tensor to the effective Young's moduli of the porous material we introduce the dimensionless parameters $\tilde{E}_1$, $\tilde{E}_2$, and $\tilde{E}_3$ defined as

$$\frac{E_i}{E_0} = \frac{1}{1+p\tilde{E}_i} \tag{4}$$

where $E_0$ is the matrix Young's modulus (note that in all our considerations we assume the matrix to be isotropic), and $E_i$ are the effective Young's moduli in three orthogonal directions. Three parameters $\tilde{E}_i$ ($i = 1, 2, 3$) characterize the change in Young's modulus in $x_i$-direction induced by the pores of the same shape in the case when these pores are parallel to each other. These parameters can be expressed in terms of the $\mathbf{H}$ -tensor components for the corresponding pore shapes:

$$\tilde{E}_i = \frac{E_0}{p} H_{iiii} \quad \text{(no summation over repeating indices)} \tag{5}$$

In most of the previous publications, the pore compliance contribution is found deterministically, either analytically for a pore in unbounded medium (Eshelby, 1957, 1959; Kachanov et al., 1994) or numerically, for example, by finite element analysis (FEA) performed on a reference volume containing an individual pore, see Tsukrov and Novak (2002), Drach et al. (2011). Numerical simulations appear to be the only option for the irregularly-shaped pores for which no analytical solutions are available. Even though the entire numerical procedure can be completely automated (see for example Drach et al., 2011), this method may not be practical when contributions of tens of thousands of different pores are to be estimated.

Our method involves statistical analysis to derive a formula predicting contribution of a pore to effective properties based on its geometric parameters. First, we run a relatively small number of FEA simulations (~100–200) for individual pores in a reference volume. The set of pores is chosen as an "optimal" subset of data using the DoE approach so that the pore shape parameters allow to obtain the model with a specified level of variance across the whole parameter space. Then a polynomial is fitted to the simulation results and estimates for the rest of the pores are inferred from the resulting empirical formula. Thus, the statistical analysis results in a polynomial approximation model, which correlates pore contributions with their geometric parameters. If $m$ geometric parameters are chosen, and the degree of approximating polynomial is $n$, the polynomial has the following general form

$$\begin{aligned} PCC = {} & \alpha_0 + \alpha_1 F_1 + \alpha_2 F_2 + \cdots + \alpha_m F_m + \alpha_{m+1} F_1^2 + \alpha_{m+2} F_2^2 + \cdots \\ & + \alpha_{n\cdot m} F_m^n + \alpha_{n\cdot m+1} F_1 \cdots F_n + \cdots + \alpha_N F_{m-n+1} \cdot F_m \end{aligned} \tag{6}$$

where $PCC$ is the predicted contribution to Young's modulus ($\tilde{E}_1$, $\tilde{E}_2$ or $\tilde{E}_3$); $F_1 \ldots F_m$ are the considered pore geometry parameters (model factors); $\alpha_0 \ldots \alpha_N$ are the coefficients determined by the standard least squares fit of FEA simulation data. In the case of a 3-factor 2nd degree model, the expression is

$$\begin{aligned} PCC = {} & \alpha_0 + \alpha_1 F_1 + \alpha_2 F_2 + \alpha_3 F_3 + \alpha_4 F_1^2 + \alpha_5 F_2^2 + \alpha_6 F_3^2 \\ & + \alpha_7 F_1 F_2 + \alpha_8 F_2 F_3 + \alpha_9 F_3 F_1 \end{aligned} \tag{7}$$

Such a statistical model can be used to predict contributions of any pore with a specific set of geometric parameters.

The examples of the model are given in Drach et al. (2013), where fitting of the FEA predictions is performed using the response surface methodology (Myers et al., 2009) based on the following geometric parameters (model factors): principal moments of inertia of each pore and its surface-to-volume ratio. In that work, the set of irregular shapes used to construct the model was obtained from a microtomography scan of a carbon/carbon composite sample. The models were constructed for pore contributions to the overall bulk, shear and Young's moduli based on 150 pores selected using the DoE approach. The models were validated on another set of 150 randomly chosen pores not included in the model. A reasonably good fit was observed for bulk and shear moduli: bulk modulus contribution $R^2 = 0.98$, $RMSE = 6.8\%$ (hereafter the mean error, $ME$ and analogously the root-mean-square error, $RMSE$, values are presented in percentages, e.g.: $ME = 100\% \cdot MeanError/MeanResponse$); shear modulus contribution $R^2 = 0.92$, $RMSE = 3.6\%$. However, the regression's fit values for Young's moduli contribution parameters were found to be lower ($R^2$ in the range of $0.75 \ldots 0.87$). Thus, it appears that the principal moments of inertia with surface-to-volume ratio are

not the most suitable combination of geometric parameters to evaluate the contribution of pores to the effective Young's moduli of porous solids.

## 3. Shape projected areas as the geometric parameters determining pore contributions to effective Young's moduli

We consider the projected areas of pores ("shadows") as a candidate set of geometric parameters for correlation with effective Young's moduli. We use the projections on three global coordinate planes in the original coordinate system of the scanned specimen (see Fig. 3) and normalize them with respect to the pore volume:

$$\tilde{A}_i = \frac{\sqrt{A_i}}{\sqrt[3]{V}} \tag{8}$$

where $A_i$ and $\tilde{A}_i$ are the initial and normalized areas of the pore projection onto the plane normal to the $x_i$th axis ($i = 1, 2, 3$), and $V$ is the volume of considered pore.

Two datasets are considered. The first dataset consists of 8351 pores obtained by processing the microcomputed tomography ($\mu$CT) data for a specimen of carbon/carbon composite, see Drach et al. (2011, 2013).

The second dataset is based on the $\mu$CT scan of a sample of 3D woven carbon/epoxy composite provided by Albany Engineered Composites (Rochester, NH). For this dataset, the reconstructed images of the sample slices in the format of 8-bit grayscale VTK were processed in the open source image processing software Fiji (see http://fiji.sc/Fiji) before pore shape extraction. First, a "Fit Polynomial" filter with parameters "3 × 3 × 3" was applied to correct for brightness variation within and across the slices. Next, the slices were binarized using "Threshold" filter with the value of "64". In the resulting binary images, white regions represent pores and black is everything else (matrix and reinforcement), see Fig. 4. The pores smaller than 3 voxels in any dimension were regarded as noise and not extracted.

The MATLAB code first described in Drach et al. (2013) was used for automatic extraction of individual pore meshes and calculation of pore geometric parameters as follows. VTK file containing series of black and white images was imported into MATLAB workspace resulting in a 3D matrix with dimensions equal to the dimensions of the VTK file. Components in the matrix have integer values: '0' for the black color and '1' for the white color corresponding to the pores. The matrix was then processed using functions from MATLAB Image Processing Toolbox to obtain information about

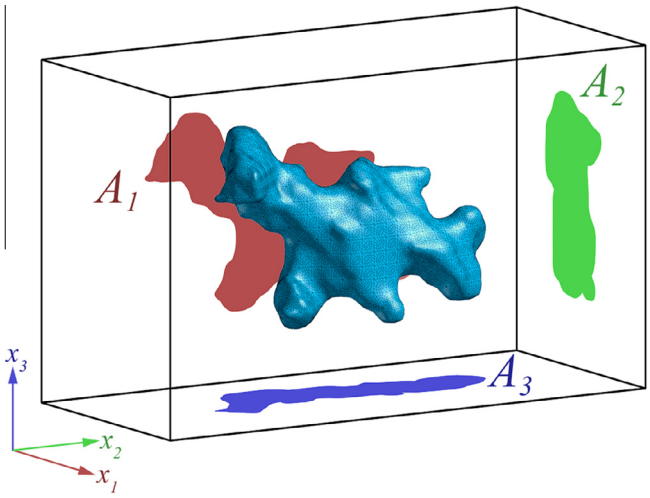


**Fig. 3.** Three projected areas ("shadows") of a pore.

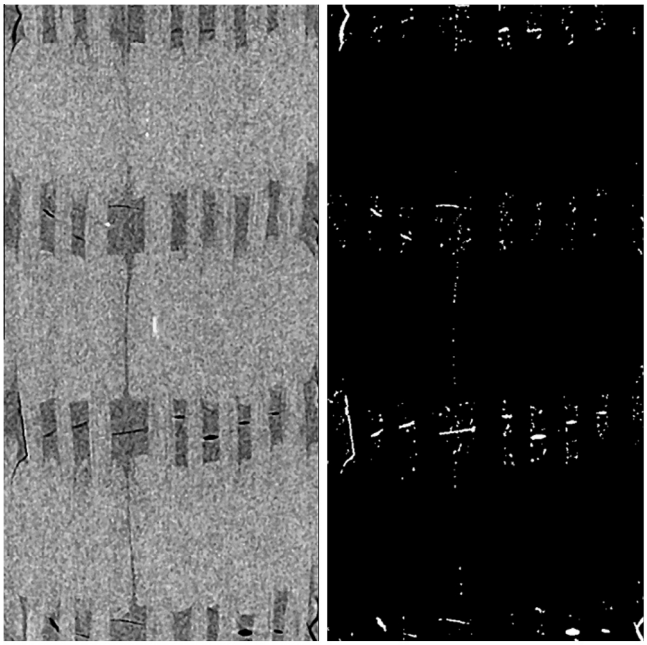


**Fig. 4.** Reconstructed images of the 3D woven composite sample slices before and after image processing in Fiji.

all connected objects (in our case, pores) in the input matrix. The information included the number of objects and the coordinates of the components in the input matrix comprising these objects. The criterion by which the components were determined to be connected to the objects was defined by the connectivity parameter. In our procedure we used the 6-connected neighborhood connectivity, meaning that the matrix component was considered to be a part of the object if it was located in the same row or column as one of the object components and is adjacent to it. In the next part of the script, individual objects were processed to determine their geometric parameters. As the result of the extraction, a triangular surface mesh was generated and a number of geometric properties were stored (e.g. linear dimensions, volume, principal moments of inertia, projected areas, etc.). The final design space contained 8351 extracted pores for carbon/carbon composite and 24,041 extracted pores for 3D woven composite. The ranges of normalized projected area parameters are given in Table 1.

The DoE approach was utilized to identify the optimal number and the combination of pores for two models (carbon/carbon and 3D woven carbon/epoxy pore sets). Using JMP software (SAS Institute Inc, 2010) we constructed a custom I-optimal experimental design with the aim of producing statistical models with minimal overall variance across the design space. The number of pores for the initial design was chosen to be 100, which corresponds to the average relative prediction variance of 0.05. The complete set of input variable is provided in Table 2.

For a finite number of pores extracted from the microtomography data, it was impossible to find pores with normalized projected areas that exactly matched the design points produced by the DoE analysis. Therefore, the pores with the smallest deviation of the parameters from the designed values were chosen. After analyzing the available pore data, it was found that the pore parameter space is bound by a constraint that the sum of the three parameters must be greater than or equal to 3.15 (note that for a sphere $\tilde{A}_1 + \tilde{A}_2 + \tilde{A}_3 = 3.3$ and for a cube with the sides parallel to the coordinate planes: $\tilde{A}_1 + \tilde{A}_2 + \tilde{A}_3 = 3.0$). This constraint is taken into account in the DoE analysis.

**Table 1**
The ranges of the three normalized projected area parameters of the pores from the carbon/carbon composite and 3D woven carbon/epoxy composite datasets.

| | Minimum value (*MIN*) | Maximum value (*MAX*) | Average value (AVG) $AVG = \frac{MAX+MIN}{2}$ | Midrange value (MID) $MID = \frac{MAX-MIN}{2}$ |
|---|---|---|---|---|
| | | *Carbon/carbon composite dataset* | | |
| $\tilde{A}_1$ | 1.03 | 1.79 | 1.41 | 0.38 |
| $\tilde{A}_2$ | 1.05 | 1.75 | 1.40 | 0.35 |
| $\tilde{A}_3$ | 0.99 | 1.59 | 1.29 | 0.30 |
| | | *3D woven carbon/epoxy composite dataset* | | |
| $\tilde{A}_1$ | 0.90 | 1.35 | 1.13 | 0.23 |
| $\tilde{A}_2$ | 1.00 | 1.43 | 1.22 | 0.22 |
| $\tilde{A}_3$ | 1.20 | 1.89 | 1.55 | 0.35 |

**Table 2**
Parameters chosen in the DoE module of JMP software.

| Parameter | Value |
|---|---|
| Input variables[a] | $\tilde{A}_1, \tilde{A}_2, \tilde{A}_3$ |
| Constraints for input variables[b] | $\tilde{A}_1 + \tilde{A}_2 + \tilde{A}_3 \geqslant 3.15$ |
| Three model responses | $\tilde{E}_1, \tilde{E}_2, \tilde{E}_3$ |
| Prediction model type | 2nd order response surface model |
| Number of experimental runs (design points) | 90 |
| Additional runs (center points) | 10 |
| Number of replicates | 0 |
| Number of random starts for search of optimal designs | 1000 |

[a] Continuous variables with ranges shown in Table 1.
[b] This constraint is applicable to the considered datasets only.

Finite element simulations were performed and results were processed to determine the components of **H** -tensor of individual pores according to the following automated procedure. Surface mesh of a pore was placed in a cube-shaped reference volume with sides five times larger than the largest dimension of the pore, see Fig. 5. This setup was auto meshed with second-order tetrahedral elements. Typical pore shapes yielded FE meshes with the number of elements on the order of 100,000. Material properties were then applied to all matrix elements. Since the results were normalized by Young's modulus of the matrix $E_0$, the value $E_0 = 1$ was used. Poisson's ratio was set to $\nu_0 = 0.33$ in this study. Six sets of boundary conditions in displacements were consecutively applied to simulate three loadcases of uniaxial tension (in the directions of three global coordinate axes) and three shear loadcases.

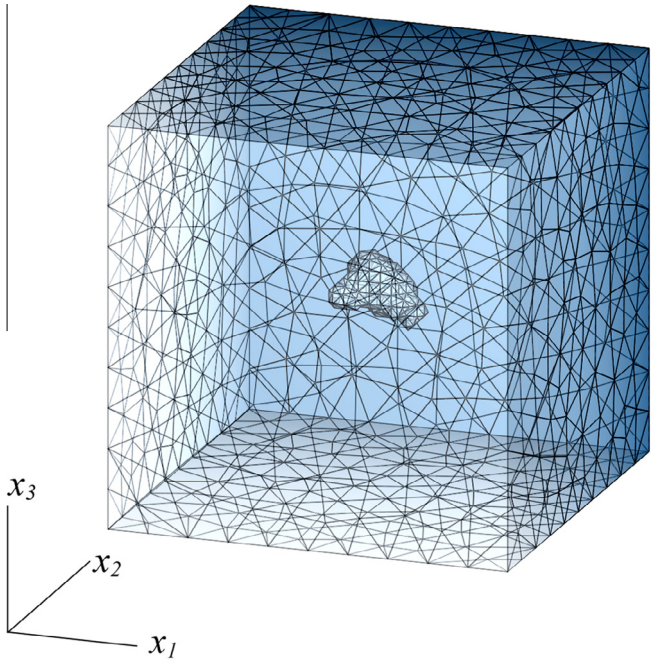


**Fig. 5.** Reference volume with a pore surface mesh inside.

The simulation results' files were processed via a custom Python script. The script computed volume averages of all stress components $\left\langle \sigma_{ij}^{(k)} \right\rangle_{RV}$ for each loadcase $k$. With the volume averages known, the pore stiffness contribution tensor $N_{ijkl}$ can be calculated: e.g. from the first loadcase (uniaxial tension in $x_1$ direction): $N_{ij11} = \left(\sigma_{ij}^{(0)} - \left\langle \sigma_{ij}^{(1)} \right\rangle_{RV}\right)/\varepsilon^{(0)}$, where $\sigma_{ij}^{(0)}$ are the stresses in the matrix material subjected to $\varepsilon_{11} = \varepsilon^{(0)}$, $\langle \sigma_{ij}^{(1)} \rangle_{RV}$ are the stress volume averages in the porous material subjected to $\varepsilon_{11} = \varepsilon^{(0)}$. Pore compliance contribution tensor $H_{ijkl}$ was then expressed in terms of $N_{ijkl}$: $H_{ijkl} = -S_{ijmn}^{(0)} N_{mnpq} S_{pqkl}^{(0)}$, where $S_{ijkl}^{(0)}$ are the components of the compliance tensor of the matrix material. Finally, parameters $\tilde{E}_1, \tilde{E}_2, \tilde{E}_3$ were calculated from the components of **H** -tensor using formula (5).

Thus, for each pore characterized by three normalized "shadow" parameters $\tilde{A}_1$, $\tilde{A}_2$, $\tilde{A}_3$, a set of three compliance contribution parameters $\tilde{E}_1, \tilde{E}_2, \tilde{E}_3$ was determined from FEA. These values were entered into JMP software for statistical analysis.

## 4. Results of the statistical analysis

The results of the statistical analysis are the sets of coefficients in expression (7) for predictions of $\tilde{E}_1, \tilde{E}_2, \tilde{E}_3$:

(a) for carbon/carbon composite dataset

$$\begin{aligned}
\tilde{E}_1 &= 2.509 + 0.844\hat{A}_1 - 0.349\hat{A}_2 - 0.195\hat{A}_3 - 0.270\hat{A}_1\hat{A}_2 - 0.106\hat{A}_1\hat{A}_3 + 0.252\hat{A}_2\hat{A}_3 \\
\tilde{E}_2 &= 2.485 - 0.362\hat{A}_1 + 0.790\hat{A}_2 - 0.201\hat{A}_3 - 0.315\hat{A}_1\hat{A}_2 + 0.212\hat{A}_1\hat{A}_3 - 0.125\hat{A}_2\hat{A}_3 \\
\tilde{E}_3 &= 2.177 - 0.219\hat{A}_1 - 0.205\hat{A}_2 + 0.561\hat{A}_3 + 0.209\hat{A}_1\hat{A}_2 - 0.174\hat{A}_1\hat{A}_3 - 0.163\hat{A}_2\hat{A}_3
\end{aligned} \tag{9a}$$

(b) for 3D woven carbon/epoxy composite dataset

$$\begin{aligned}
\tilde{E}_1 &= 1.873 + 0.392\hat{A}_1 - 0.079\hat{A}_2 - 0.184\hat{A}_3 - 0.053\hat{A}_1\hat{A}_2 - 0.101\hat{A}_1\hat{A}_3 + 0.064\hat{A}_2\hat{A}_3 \\
\tilde{E}_2 &= 2.086 - 0.092\hat{A}_1 + 0.417\hat{A}_2 - 0.253\hat{A}_3 - 0.065\hat{A}_1\hat{A}_2 + 0.072\hat{A}_1\hat{A}_3 - 0.104\hat{A}_2\hat{A}_3 \\
\tilde{E}_3 &= 3.317 - 0.226\hat{A}_1 - 0.267\hat{A}_2 + 1.148\hat{A}_3 + 0.227\hat{A}_1\hat{A}_2 - 0.153\hat{A}_1\hat{A}_3 - 0.222\hat{A}_2\hat{A}_3
\end{aligned} \tag{9b}$$

where $\hat{A}_i = \frac{\tilde{A}_i - AVG(\tilde{A}_i)}{MID(\tilde{A}_i)}$ (see Table 1).

In these models the insignificant factors with $p$-values ($p$-value is the probability that the factor coefficient value is different from zero due to random error) higher than the level of significance of 0.01 are excluded sequentially by removing one insignificant parameter at a time and re-running the model. In both models, the 2nd degree single factor parameters turned out to be insignificant, while interaction components were significant in all responses.

Graphically the results for both models are presented in Fig. 6. In these plots, the straight line represents the perfect fit when the model predicted values coincide with the actual values (*Actual* = *Predicted*, where the term "Actual" is used for the results of direct FEA simulations). The two curves below and above the straight line represent the 95% confidence intervals for the predicted values. In the case of carbon/carbon composite dataset, the correlation coefficients and root-mean-square errors for $\tilde{E}_1$, $\tilde{E}_2$, $\tilde{E}_3$ are a $R^2 = 0.96, 0.95, 0.96$ and $RMSE = 5.1\%, 5.5\%, 3.9\%$, correspondingly. In the case of carbon/epoxy dataset, $R^2 = 0.96, 0.93, 0.97$ and $RMSE = 3.2\%, 4.3\%, 4.4\%$. Thus, we conclude that a good correlation is observed between the normalized "shadow" parameters and Young's moduli pore contribution parameters.

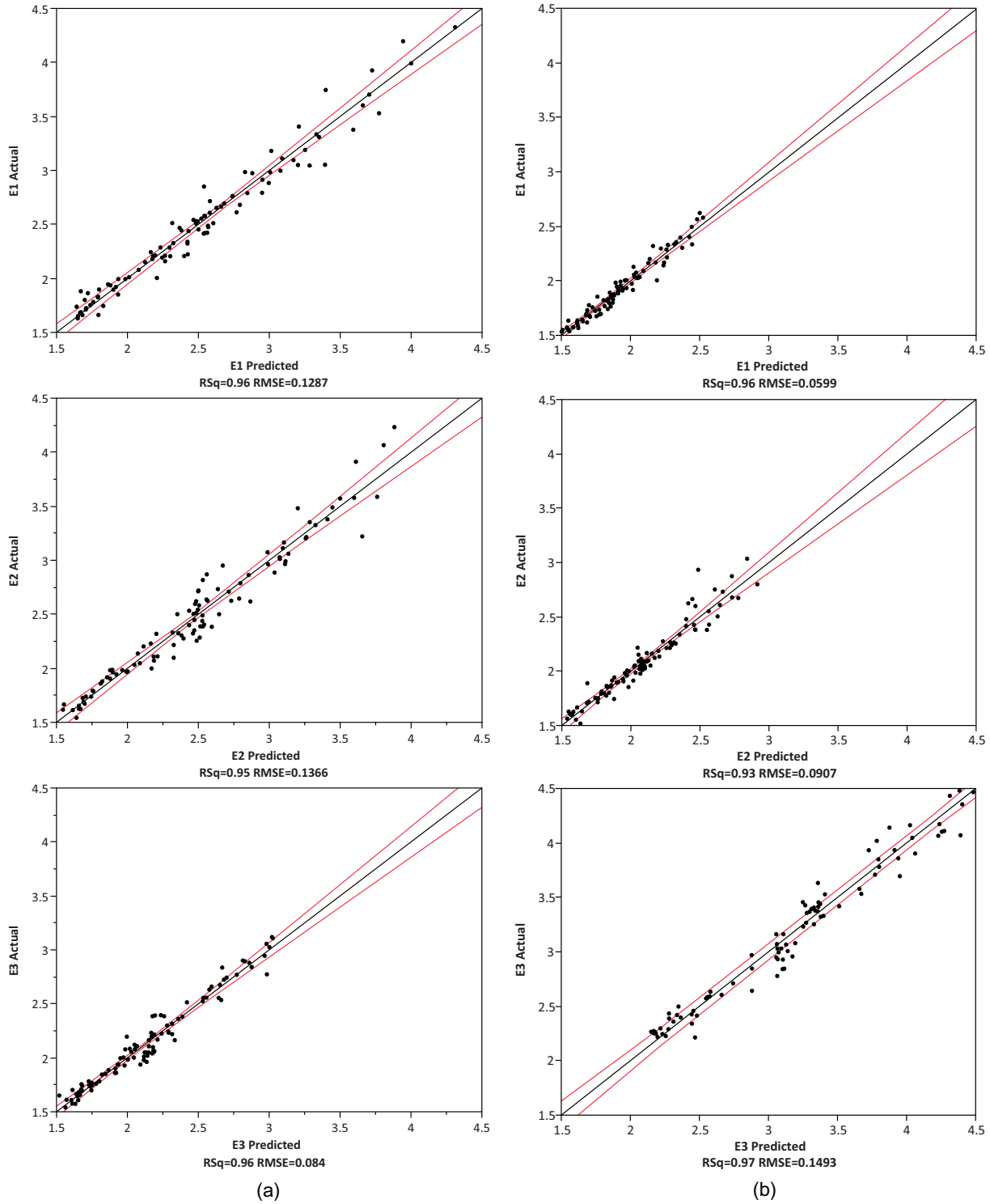


**Fig. 6.** The results of response surface fitting presented as plots of direct calculation results ($\tilde{E}_i$ *Actual*) vs. model prediction results ($\tilde{E}_i$ *Predicted*) for pore compliance contribution parameters: (a) carbon/carbon composite dataset; (b) 3D woven carbon/epoxy composite dataset.

For validation of the proposed stochastic 3-factor PCC model given by formulae (9), the estimates of pore compliance contribution parameters for each dataset were compared to the direct FEA simulations performed on an independently chosen set of 100 pores which were not used for the model development. For this experiment, the normalized projected area parameters were selected randomly with uniform distribution over the design space. Pore geometries were selected from the original datasets with all available pores. The results of the validation experiment are shown in Fig. 7. The values of $R^2$ and *RMSE* for carbon/carbon composite are $R^2 = 0.96, 0.95, 0.92$ and $RMSE = 4.6\%, 4.7\%, 5.3\%$ for $\tilde{E}_1$, $\tilde{E}_2$ and $\tilde{E}_3$ responses, correspondingly. For 3D woven carbon/epoxy composite, the values of $R^2$ and *RMSE* are $R^2 = 0.96, 0.92, 0.94$ and $RMSE = 2.7\%, 4.0\%, 4.7\%$ for $\tilde{E}_1$, $\tilde{E}_2$ and $\tilde{E}_3$ responses,

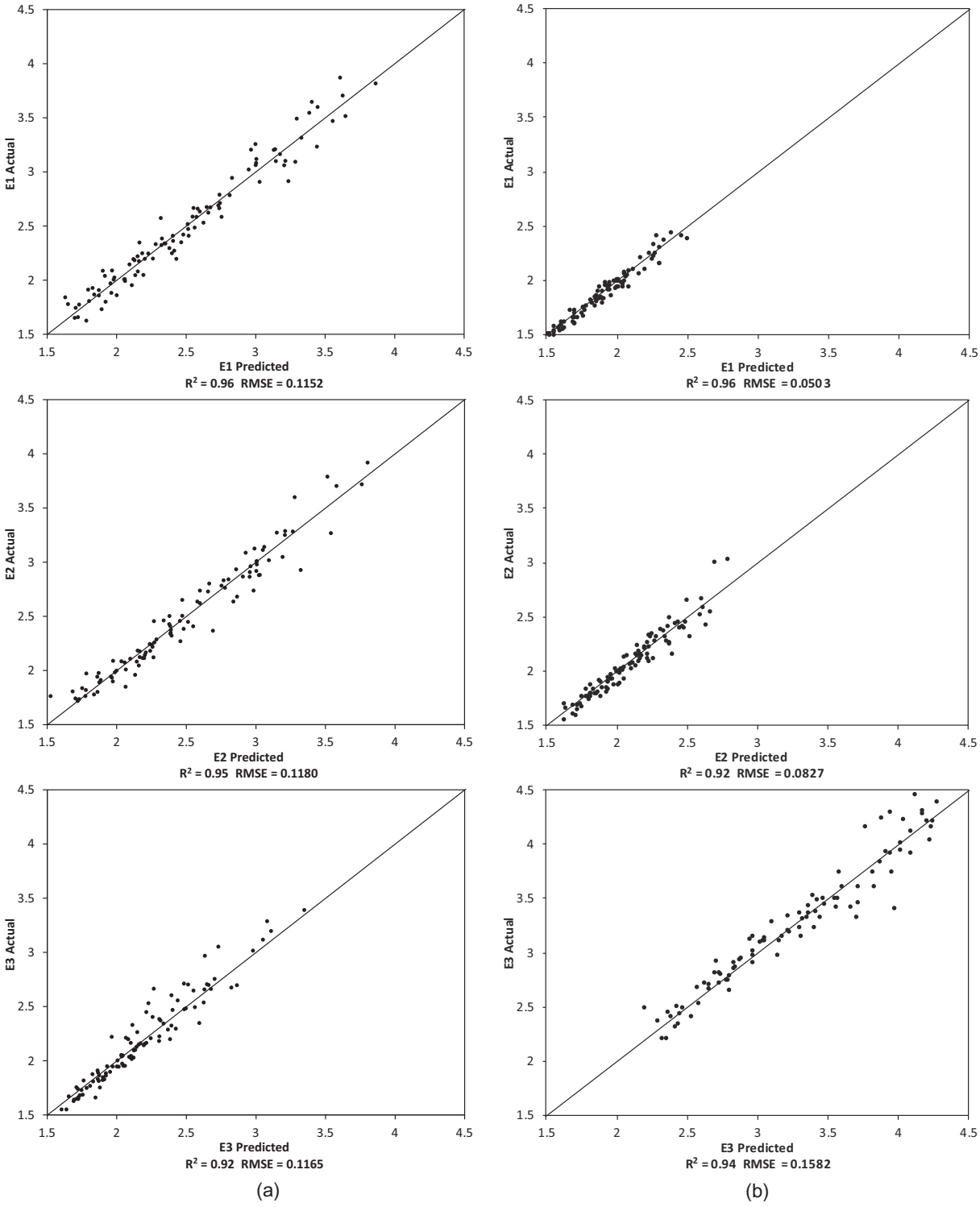


**Fig. 7.** Validation of the statistical model for responses $\tilde{E}_1$, $\tilde{E}_2$ and $\tilde{E}_3$ performed on 100 pores not included in the original model: (a) carbon/carbon composite dataset; (b) 3D woven carbon/epoxy composite dataset.

correspondingly. These results indicate that the proposed models can be used to estimate with reasonable accuracy the pore compliance contribution parameters of the remaining 8251 pores in the carbon/carbon composite dataset and 23,941 pores in the carbon/epoxy dataset that were not included in the original experiments.

The accuracy of the 3-factor model (based on the projected areas) for the carbon/carbon composite dataset can be compared to the 4-factor model (based on the principal moments of inertia and surface-to-volume ratio) presented in Drach et al. (2013). The mean errors from the validation studies for predictions of $\tilde{E}_1$, $\tilde{E}_2$ and $\tilde{E}_3$ are correspondingly −0.1%, 0.2%, −0.4% for 3-factor model, and −3.5%, −3.0% 1.9% for 4-factor model. Similarly, the root-mean-square error values are 4.6%, 4.7%, 5.3% for 3-factor model, and 8.0%, 7.7%, 11.1% for 4-factor model. It can be seen that both the bias (mean error) and the scatter (RMSE) are lower for the model constructed using the normalized projected areas. We conclude that for the considered carbon/carbon composite dataset, the choice of projected areas as the model factors provides more

**Table 3**
Summary of data on accuracy of the considered statistical models.

| Model | $E_1$ | | | $E_2$ | | | $E_3$ | | |
|---|---|---|---|---|---|---|---|---|---|
| | $R^2$ | *ME* | *RMSE* | $R^2$ | *ME* | *RMSE* | $R^2$ | *ME* | *RMSE* |
| 4-factor model (Drach et al., 2013) | 0.87 | 0.0000 (0.0%) | 0.0805 (5.0%) | 0.75 | 0.0000 (0.0%) | 0.1084 (5.5%) | 0.82 | 0.0000 (0.0%) | 0.2836 (10.0%) |
| 4-factor model validation (Drach et al., 2013) | 0.69 | −0.0607 (−3.5%) | 0.1389 (8.0%) | 0.55 | −0.0614 (−3.0%) | 0.1579 (7.7%) | 0.55 | 0.0536 (1.9%) | 0.3106 (11.1%) |
| Proposed 3-factor model (carbon/carbon dataset) | 0.96 | 0.0000 (0.0%) | 0.1287 (5.1%) | 0.95 | 0.0000 (0.0%) | 0.1366 (5.5%) | 0.96 | 0.0000 (0.0%) | 0.084 (3.9%) |
| Proposed 3-factor model validation (carbon/carbon dataset) | 0.96 | −0.0030 (−0.1%) | 0.1152 (4.6%) | 0.95 | 0.0040 (0.2%) | 0.1180 (4.7%) | 0.92 | −0.0082 (−0.4%) | 0.1165 (5.3%) |
| Proposed 3-factor model (3D woven carbon/epoxy dataset) | 0.96 | 0.0000 (0.0%) | 0.0599 (3.2%) | 0.93 | 0.0000 (0.0%) | 0.0907 (4.3%) | 0.97 | 0.0000 (0.0%) | 0.1493 (4.4%) |
| Proposed 3-factor model validation (3D woven carbon/epoxy dataset) | 0.96 | 0.0044 (0.2%) | 0.0503 (2.7%) | 0.92 | 0.0024 (0.1%) | 0.0827 (4.0%) | 0.94 | −0.0393 (−1.2%) | 0.1582 (4.7%) |

accurate predictions of effective Young's moduli as compared to the model based on the principal moments of inertia and surface-to-volume ratio. Note that another drawback of the 4-factor model is that orientation of the pore principal axes needs to be in the direction of the global axes, otherwise we would need to include orientation vectors in the model. In the model based on "shadows", no such adjustment is necessary. Table 3 summarizes the data on accuracy of predicting the pore contributions to the overall Young's moduli based on 4 parameters (principal moments of inertia and the surface-to-volume ratio) and 3 parameters (normalized projected areas).

## 5. Conclusions

A statistical model based on the normalized projected area parameters is proposed for correlation of geometry of irregularly shaped pores with their contributions to the effective Young's moduli of the porous material. The model is applied to large data sets of pores in two different composite materials. The Young's moduli in three orthogonal directions coinciding with the global coordinate system of the specimens are considered. In each case, one hundred pores were selected to construct the corresponding models. Design of experiments techniques were utilized to select the pores producing minimal variability of model predictions across the entire factor space. The constructed models for three Young's moduli parameters $\tilde{E}_1, \tilde{E}_2, \tilde{E}_3$ have high values of $R^2$ in both material systems (0.96, 0.95, 0.96 in carbon/carbon composite model, and 0.96, 0.93, 0.97 in 3D woven carbon/epoxy composite model), as well as relatively low values of *RMSE* (5.1%, 5.5% and 3.9% in carbon/carbon composite model and 3.2%, 4.3% and 4.4% in 3D woven carbon/epoxy composite model). These results indicate that the proposed models, created based on 100 pore shapes in each case, can be used to estimate with reasonable accuracy the Young's moduli contribution parameters $\tilde{E}_1$, $\tilde{E}_2$ and $\tilde{E}_3$ for large data sets of pores, in our case more than 8000 in a sample of carbon/carbon composite and more than 24,000 in a sample of 3D woven carbon/epoxy composite. One of the advantages of the proposed method is that each pore is considered in the global coordinate system of the specimen. In contrast to most presently used micromechanical approaches, there is no need for solving the elasticity problem in the coordinate system associated with the pore followed by the coordinate transformation to the global coordinate system. Thus, the only information needed to evaluate the pore's contribution to effective Young's moduli is its projected areas in the global coordinate system.

## Acknowledgements

The authors gratefully acknowledge the financial support of the National Science Foundation through the grants DMR-0806906 and CMMI-1100409. The microcomputed tomography data was provided by Karlsruhe Institute of Technology (carbon/carbon composite) and Albany Engineered Composites, Inc. (3D woven carbon/epoxy composite). The New Hampshire Innovation Research Center is acknowledged for initial support of the collaboration between the University of New Hampshire and Albany Engineered Composites, Inc.

The authors would like to thank Philip Ramsey for valuable discussions on statistical analysis and design of experiment methodologies. The authors also express their gratitude to Robert Zimmerman for his insightful comments on compressibility and overall elastic behavior of irregular pores. Andrew Drach gratefully acknowledges the financial support provided by the ICES Postdoctoral Fellowship.

## References

Arns, C.H., Knackstedt, M.A., Pinczewski, W.V., Garboczi, E.J., 2002. Computation of linear elastic properties from microtomographic images: methodology and agreement between theory and experiment. J. Geophys. 67, 1396–1405.
Benveniste, Y., 1987. A new approach to the application of Mori–Tanaka's theory in composite materials. Mech. Mater. 6, 147–157.
David, E.C., Zimmerman, R.W., 2011. Elastic moduli of solids containing spheroidal pores. Int. J. Eng. Sci. 49, 544–560.
Dewey, J.M., 1947. The elastic constants of materials loaded with non-rigid fillers. J. Appl. Phys. D9, 665–675.
Drach, B., Tsukrov, I., Gross, T., Dietrich, S., Weidenmann, K., Piat, R., Böhlke, T., 2011. Numerical modeling of carbon/carbon composites with nanotextured matrix and 3D pores of irregular shapes. Int. J. Solids Struct. 48, 2447–2457.
Drach, B., Drach, A., Tsukrov, I., 2013. Characterization and statistical modeling of irregular porosity in carbon/carbon composites based on X-ray microtomography data. J. Appl. Math. Mech. 93, 346–366.
Ekneligoda, T.C., Zimmerman, R.W., 2006. Compressibility of two-dimensional pores having *n*-fold axes of symmetry. Proc. R. Soc. A Math. Phys. Eng. Sci. 462, 1933–1947.
Ekneligoda, T.C., Zimmerman, R.W., 2008a. Boundary perturbation solution for nearly circular holes and rigid inclusions in an infinite elastic medium. J. Appl. Mech. 75.
Ekneligoda, T.C., Zimmerman, R.W., 2008b. Shear compliance of two-dimensional pores possessing *N*-fold axis of rotational symmetry. Proc. R. Soc. A Math. Phys. Eng. Sci. 464, 759–775.
Eroshkin, O., Tsukrov, I., 2005. On micromechanical modeling of particulate composites with inclusions of various shapes. Int. J. Solids Struct. 42, 409–427.
Eshelby, J.D., 1957. The determination of the elastic field of an ellipsoidal inclusion, and related problems. Proc. R. Soc. A Math. Phys. Eng. Sci. 241, 376–396.
Eshelby, J.D., 1959. The elastic field outside an ellipsoidal inclusion. Proc. R. Soc. London Ser. A Math. Phys. Sci. 252, 561–569.
González, C., Segurado, J., LLorca, J., 2004. Numerical simulation of elasto-plastic deformation of composites: evolution of stress microfields and implications for homogenization models. J. Mech. Phys. Solids 52, 1573–1593.
Hashemi, R., Avazmohammadi, R., Shodja, H.M., Weng, G.J., 2009. Composites with superspherical inhomogeneities. Philos. Mag. Lett. 89, 439–451.
Hashin, Z., Shtrikman, S., 1962. On some variational principles in anisotropic and nonhomogeneous elasticity. J. Mech. Phys. Solids 10, 78–96.
Hill, R., 1963. Elastic properties of reinforced solids: some theoretical principles. J. Mech. Phys. Solids 11, 357–372.
Hill, R., 1965. A self-consistent mechanics of composite materials. J. Mech. Phys. Solids 13, 213–222.
Horii, H., Nemat-Nasser, S., 1983. Overall moduli of solids with microcracks: load-induced anisotropy. J. Mech. Phys. Solids 31, 155–171.

Jasiuk, I., Chen, J., Thorpe, M., 1994. Elastic moduli of two dimensional materials with polygonal and elliptical holes. Appl. Mech. Rev. 47, 18–28.
Kachanov, M., Sevostianov, I., 2005. On quantitative characterization of microstructures and effective properties. Int. J. Solids Struct. 42, 309–336.
Kachanov, M., Tsukrov, I., Shafiro, B., 1994. Effective moduli of solids with cavities of various shapes. Appl. Mech. Rev. 47, S151.
Lee, J.K., Johnson, W.C., 1978. Calculation of the elastic strain field of a cuboidal precipitate in an anisotropic matrix. Phys. Status Solidi A 46, 267–272.
Li, M., Ghosh, S., Richmond, O., 1999. An experimental–computational approach to the investigation of damage evolution in discontinuously reinforced aluminum matrix composite. Acta Mater. 47, 3515–3532.
Lubarda, V.A., Markenscoff, X., 1998. On the absence of Eshelby property for non-ellipsoidal inclusions. Int. J. Solids Struct. 35, 3405–3411.
Mackenzie, J.K., 1950. The elastic constants of a solid containing spherical holes. Proc. Phys. Soc. (London) 63B, 2–11.
Mori, T., Tanaka, K., 1973. Average stress in matrix and average elastic energy of materials with misfitting inclusions. Acta Metall. 21, 571–574.
Myers, R.H., Montgomery, D.C., Anderson-Cook, C.M., 2009. Response Surface Methodology: Process and Product Optimization using Designed Experiments, third ed. John Wiley and Sons, Hoboken, NJ.
Nemat-Nasser, S., Hori, M., 1999. Micromechanics: Overall Properties of Heterogeneous Solids, second ed. Elsevier Science Publishers.
Nozaki, H., Taya, M., 1997. Elastic fields in a polygon-shaped inclusion with uniform eigenstrains. J. Appl. Mech. 64, 495–502.
Onaka, S., 2001. Averaged Eshelby tensor and elastic strain energy of a superspherical inclusion with uniform eigenstrains. Philos. Mag. Lett. 81, 265–272.
Roberts, A.P., Garboczi, E.J., 2000. Elastic properties of model porous ceramics. J. Am. Ceram. Soc. 83, 3041–3048.
Rodin, G., 1996. Eshelby's inclusion problem for polygons and polyhedra. J. Mech. Phys. Solids 44, 1977–1995.
Ryan, T.P., 2007. Modern Experimental Design. John Wiley & Sons, Hoboken, NJ.
SAS Institute Inc, 2010. JMP 9 Design of Experiments Guide. SAS Institute Inc, Cary, NC. <www.jmp.com/support/downloads/pdf/jmp902/doe_guide.pdf> (retrieved 28.09.11).
Sevostianov, I., Giraud, A., 2012. On the compliance contribution tensor for a concave superspherical pore. Int. J. Fract. 177, 199–206.
Tsukrov, I., Kachanov, M., 1993. Solids with holes of irregular shapes: effective moduli and anisotropy. Int. J. Fract. 64, R9–R12.
Tsukrov, I., Novak, J., 2002. Effective elastic properties of solids with defects of irregular shapes. Int. J. Solids Struct. 39, 1539–1555.
Wu, T.Te., 1966. The effect of inclusion shape on the elastic moduli of a two-phase material. Int. J. Solids Struct. 2, 1–8.
Zimmerman, R.W., 1986. Compressibility of two-dimensional cavities of various shapes. J. Appl. Mech. 53, 500–504.
Zimmerman, R.W., 1991. Compressibility of Sandstones. Elsevier.
Zou, W., He, Q., Huang, M., Zheng, Q.-S., 2010. Eshelby's problem of non-elliptical inclusions. J. Mech. Phys. Solids 58, 346–372.